Hindawi
Advances in Materials Science and Engineering
Volume 2019, Article ID 3832873, 9 pages
https://doi.org/10.1155/2019/3832873

Research Article

Mechanical Properties Optimization of Friction Stir Welded Lap Joints in Aluminium Alloy

Antonio Viscusi, Antonello Astarita, and Umberto Prisco

Department of Chemical, Materials and Production Engineering, University of Napoli Federico II, Piazzale Tecchio 80, 80125 Napoli, Italy

Correspondence should be addressed to Umberto Prisco; umberto.prisco@unina.it

Received 7 November 2018; Revised 18 January 2019; Accepted 28 January 2019; Published 17 February 2019

Guest Editor: Dariusz Rozumek

This work focuses on the influence of the rotational and travel speed on the strength of AA 2024 T3 friction stir welded lap joints. Tensile tests were carried out on minispecimens extracted from different welding zones. A central composite design was applied to identify the relative importance of the variable factors' effects and their interaction on yield/ultimate strength and elongation for both the heat affected-zone (HAZ) and nugget zone. Surface methods and gradient algorithms were used to optimize the yield strength of the joints. Shear and microhardness tests were executed to achieve a more complete mechanical characterization.

1. Introduction

The feasibility of replacing the riveting process with friction stir welding (FSW) technology in the assembly of fuselage skin-stiffener panels was the objective of several scientific papers in the last decades [1–6]. The potential of FSW to result in significantly lower assembly times and manufacturing costs, yet higher productivity, cannot be overemphasized. However, commercial applications of this process require addressing issues such as strength analysis and design as well as optimizing the manufacturing process parameters for more reliable welds with minimum distortion [7, 8]. One of the many experimental strategies used to determine the process parameters as well as to optimize the process is defined "by trial" and relies on the researcher's technical and theoretical process knowledge [9]. This strategy consists of a sequential procedure wherein the value of just one parameter among the set of parameters identified in the previous experiment is varied. This specific parameter is the one that mostly influences the process response while keeping fixed the level of the other parameters [10]. Such an approach has at least two disadvantages: it lacks objectivity in determining mathematical relations between process inputs and response variables and it also lacks efficiency and accuracy in optimizing the surface response through trials [11]. Another experimental strategy is the "one factor per time approach," wherein the researcher subsequently varies the levels of each factor within its range while keeping fixed at the base level the other factors [12]. Obviously, this approach lacks information about the factors' interactions, but it enables estimating main factors' effects. In any event, the one factor per time approach is less accurate and less efficient than the statistical approach [13]. Many studies of experimental strategies prove that the correct experimental strategy for problems involving more than one factor and data points affected by experimental errors must be taken from design of experiments (DOE) techniques if the aim is to remove objective results from experimental data [14]. These techniques allow maximum conclusive information to be drawn from minimum work, time, energy, money, or other limited resources. So, DOE aims to maximize information per run by choosing a reduced number of input sample points. Moreover, it enables developing a robust process, i.e., a process that minimizes the influence of noise variables [15]. Data organized by DOE allow the most powerful use of analysis of variances, since main factor and interaction effects can be estimated to determine their significance. Another considerable advantage of using these techniques

involves combining DOE with response surface methodologies (RSMs), more efficiently to evaluate the effectiveness of investigative trade-offs [16]. One of the most important advantages of using DOE techniques is extrapolation [17]. This property is significant because it allows optimum prediction even if "optimum" lies outside the initial design range, and the number of runs must be reduced to achieve optimum. Good predictive properties allow DOE association with other complex mathematical methods without compromising accuracy and assuring the method of steepest ascent. This method is a viable technique for sequentially moving toward the optimum response [18]. A comprehensive recitation of additional advantages of these DOE techniques is beyond the scope of this paper. Several papers deal with the influence of process parameters on properties of FSW joints [19–22]; in particular, it was adopted a DOE to investigate such influence [23]. From the literature, it is also evident that the main process parameters that need to be investigated are the rotational speed and travel speed [24–26]. In particular, it was proved that the inverse of travel speed measurements was better than travel speed to fit experimental data [27]. Therefore, this study examined the strength of FSW aluminium alloy lap joints in two different welding zones: HAZ and nugget zone. Aiming to test separately the tensile strength of HAZ and nugget zone, minispecimens from both these zones were subjected to shear and microhardness tests. The process parameters optimization issue was approached using central factorial design, response surface methods, and gradient algorithms.

2. Materials and Methods

AA 2024 T3 sheets were used as the bottom and the top sheet of the lap joints. The nominal weight percent composition (major alloying additions) of AA 2024 is 4.4% Cu, 1.5% Mg, 0.6% Mn, and the rest is aluminium. Sheets' thickness is 1.27 mm. The ultimate tensile strength (UTS) of the AA 2024 T3 base metal is 475 MPa. As for the welding process parameters, the inverse of travel speed (TS^{-1}) ranged from 0.155 to 0.533 s/mm and the rotational speed (RS) ranged from 950 to 2222.5 rpm. Plunge depth was fixed to 2.11 mm, tilt angle to zero degree, and travel angle to one degree.

Nine different TS^{-1}-RS combinations were used for obtaining 13 welds in this study; five combinations were derived by 2^2 factorial design with five centre points, and the remaining four combinations were obtained by using the steepest ascent algorithm. One tool configuration equipped with a pin consisting of a threaded frustum of the cone was used; the lower and the upper diameters are 2.77 mm and 5.06 mm, respectively, with a length of 2.03 mm. The shoulder diameter is 12.04 with a concavity of 7°. Two different machines were used to perform FSW lap and overlap joints with single pass. A controlled numerical machine (CNM) was employed to perform the set of runs concerned with the central factorial design featured by high heat generation (hot runs); a vertical milling machine was used to carry out the set of runs concerned with the steepest algorithm featured by low heat generation (cold runs).

Both the top and bottom sheets, 152.40 mm long and 2.54 mm thick, were positioned as shown in Figure 1. Sheets were degreased prior to welding using acetone as a cleaner. After the FSW process, an optical specimen was taken out from each run; microscope observations of the cross sections were carried out to identify the exact position of the welding zones. At the same time, the cross sections of the welds were observed and analysed by image processing software to identify the position of the hook defects and measure the grain size. According to ASTM E 112, the grain size number is determined by using the general intercept method. For this purposes, standard metallographic polishing procedures were used with modified Keller's reagent. Thanks to the aforementioned analyses, it was possible to remove three minitensile specimens from both the nugget and heat-affected zones for each run by using a minimilling machine.

Minitensile testing was carried out by following design of experiments. Figure 2 shows the minitensile specimen drawing with its geometrical dimensions. It is worth to note that smaller is the specimen higher are the mechanical properties recorded; experimental results of minitensile samples refer to local properties of the material which exceed the global ones [28]. Each sample was pulled out from the lap joints; then, it was refined and polished on both sides by using abrasive papers of 30 μm and 12 μm removing exceeding material and leading the thickness from 1 mm to 0.50 mm. Abrasive papers of 9 μm and 3 μm were used to eliminate the surface scratches; finally, a diamond suspension of 1 μm was used to create a like-mirror surface. The waiting time between the welding and the minitensile testing was typically 150 h. The minitensile testing was performed through a minitensile testing machine by imposing a strain rate equal to $10^{-3}\,s^{-1}$. The ultimate strength, the yield strength, and the elongation of the weld were measured. The last property was evaluated by using the Epsilon ONE optical high-precision extensometer, which is a noncontact device able to measure accurately the strain of this type of minitensile specimen at the narrow section.

The mechanical characterization of the lap joints obtained by FSW technology also included shear testing and microhardness measurements. The strength of the lap joints loaded nominally in overlap shear was examined, even though in this case, 150 h elapsed before shear testing was carried out. All the specimens tested were 25.4 mm wide, 127 mm long, and 2.54 mm thick (Figure 3), manufactured using a shear machine, and ground on both sides by milling. Three specimens for each run were tested, and the failure loads were averaged. All overlap shear tests were performed using the same strain rate used in the tensile testing. The maximum loads (failure loads) were recorded for each specimen. Each weld was sectioned and polished so the hardness could be measured using a digital Vickers hardness tester. The centre of the welds was tested throughout the cross section with 1 mm spacing between data points; all welding zones down to the base material were involved.

As for the experiments design, the central composite design (CCD), able to fit the response surface through a quadratic regression model, was used in this study. CCD contains an embedded factorial or fractional factorial design

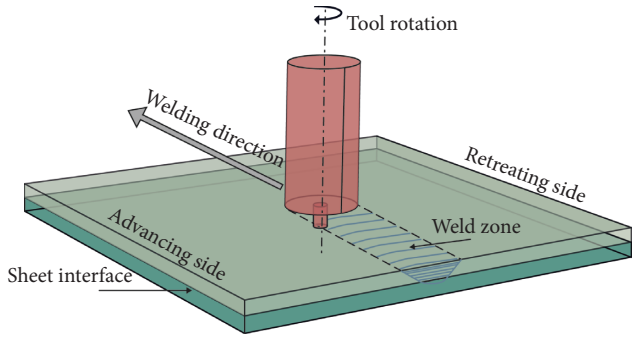

Figure 1: Schematic of friction stir welding.

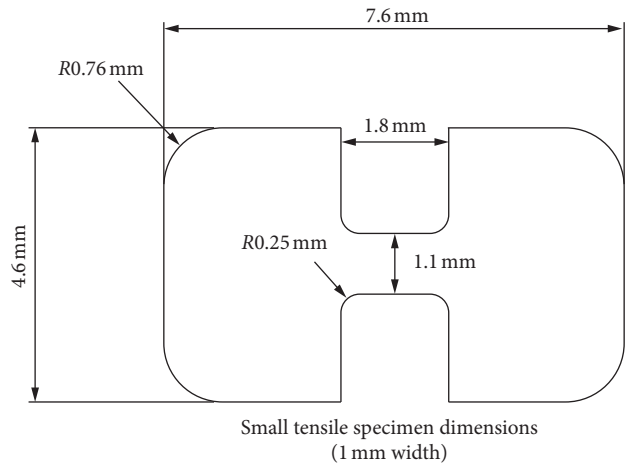

Figure 2: Minitensile specimen drawing.

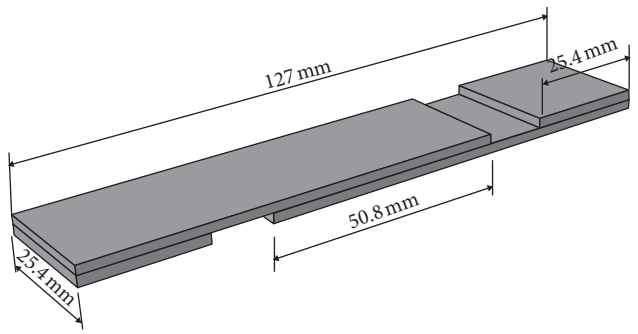

Figure 3: Shear specimens drawing.

with centre points that are augmented with a group of "star points." The importance of the centre points is that they allow for a curvature estimation [29]. The CCD could be implemented more easily with a sequential procedure: firstly, a factorial design with centre points should be performed to estimate the significance of the main factor effects and interaction effects, and above all to prove or to reject the presence of a curvature. Then, if the presence of the curvature is proved, the "star points" procedure can be performed. According to the aforementioned procedure, a 2^2 factorial design with five centre points and three repeated measurements was carried out to perform tensile testing for the nugget zone and for the heat-affected zone. The experimental table is summarized (Table 1).

Table 1: Table data for two factorial designs with five centre points.

Runs order	rpm	s/mm
1	1377.5	0.267
7	2222.5	0.267
6	1377.5	0.533
5	2222.5	0.533
2	1800.0	0.400
3	1800.0	0.400
4	1800.0	0.400
9	1800.0	0.400
8	1800.0	0.400

To avoid systematic errors, the whole set of experiments has been randomized. To perform an ANOVA in every possible case, even in the case of heteroskedasticity of data (i.e., not constant variance), a weighted ANOVA was carried out [30]. Such analysis requires repeated measurements for each run. Experimental data of yield strength, ultimate strength, and elongation are analysed and plotted separately. MINITAB, one of the most common statistical software packages, was used to define the DOE table and to perform a weighted ANOVA as well as residuals analysis. Experiments included repeats of the response, whose measurements allowed variability analysis in response data through a weighted regression. Such a method is suitable for handling data with different variances.

3. Results and Discussion

Experimental data of yield strength are shown in Table 2. An important point is that the column called WGTS_ADJ contains weights, i.e., an estimate of the reciprocal variance of the mean. These weights are due to the analysis of variability that is shown in Table 3. This analysis calculates and stores the standard deviations of the repeated responses detecting differences or dispersion effects across factor settings. This analysis even allows weights to be stored to perform a weighted ANOVA.

This analysis shows that only two effects could be considered significant: rpm with a p value of 0.094 and the inverse of the travel speed with a p value of 0.055; the interaction effect seems not to be noticeable. Neither curvature could be considered significant. The weighted ANOVA related to the experimental data of yield strength is shown in Table 4. The regression model has been reduced by removing the interaction effect since a previous analysis proved its negligibility; in fact, the value of F related to the interaction effect is 0.09 corresponding to a p value of 0.782.

The analysis shows a curvature p value of 0.145 that cannot be able to prove its presence and a main effect p value of 0.040 that ensures a significant influence; specifically, the p value related to rpm is 0.0045, and the p value related to TS^{-1} is 0.0055. Both the values can be considered significant. Regression model coefficients are estimated as shown in Table 4. Aiming to prove the model adequacy, residuals analysis was performed that is not here reported for the sake of brevity. Such an analysis verified the hypothesis made on the residuals; i.e., residuals can be assumed to be normally

Table 2: Yield strength experimental responses.

rpm	s/mm	Ys1	Ys2	Ys3	Ys4	Std. Ys	Dim	Avg. Ys	WGTS_ADJ
1377.5	0.267	372	365	353	—	9.609	3	363.333	0.0390
2222.5	0.267	361	323	356	—	20.648	3	346.667	0.0084
1377.5	0.533	349	319	368	—	24.705	3	345.333	0.0059
2222.5	0.533	402	345	249	343	63.373	4	334.750	0.0011
1800.0	0.400	353	356	326	—	16.523	3	345.000	0.0063
1800.0	0.400	356	374	320	—	27.495	3	350.000	0.0063
1800.0	0.400	360	366	348	—	9.165	3	358.000	0.0063
1800.0	0.400	342	357	397	338	26.938	4	358.500	0.0084
1800.0	0.400	355	343	392	—	25.541	3	363.333	0.0063

Table 3: Results of yield strength analysis of variability.

Regression estimated effects and coefficients for natural log of std. Ys ratio (coded units)						
Term	Effect	Effect	Coef.	SE coef.	T	p
Constant	—	—	3.0796	0.1407	21.89	0.0
rpm	0.8733	2.395	0.4367	0.2118	2.06	0.094
s/mm	1.0527	2.865	0.5264	0.2118	2.49	0.055
rpm ∗ s/mm	0.1084	1.115	0.0542	0.2118	0.26	0.808
	$R^2 = 72.04\%$		$R^2(\text{adj}) = 55.26\%$			
Analysis of variance for natural log of std. Ys						
Source	DF	Seq. SS	Adj. SS	Adj. MS	F	p
Main effects	2	6.319	5.900	2.950	5.981	0.047
2-Way interactions	1	0.032	0.032	0.032	0.070	0.808
Residual error	5	2.465	2.465	0.493	—	—
Curvature	1	0.130	0.130	0.130	0.222	0.661
Pure error	4	2.335	2.335	0.583	—	—
Total	8	8.816	—	—	—	—

Table 4: Results of yield strength weighted analysis of variance.

Estimated effects and coefficients for avg. Ys (coded units)						
Term		Effect	Coef.	SE coef.	T	p
Constant		—	346.718	3.953	87.71	0.0
rpm		−15.948	−7.974	3.004	−2.65	0.0045
s/mm		−17.026	−8.513	3.413	−2.49	0.0055
Ct Pt		—	8.469	4.903	1.73	0.45
		$S = 0.533470$	$R^2 = 73.27\%$	$R^2(\text{adj}) = 57.24\%$		
Analysis of variance for avg. Ys (coded units)						
Source	DF	Seq. SS	Adj. SS	Adj. MS	F	p
Main effects	2	3.051	3.709	1.855	6.52	0.040
Curvature	1	0.849	0.850	0.850	2.98	0.145
Residual error	5	1.423	1.422	0.285	—	—
Lack of fit	1	0.031	0.030	0.030	0.09	0.782
Pure error	4	1.393	1.392	0.348	—	—
Total	8	5.327	—	—	—	—
Estimated coefficients for avg. Ys using data in uncoded units						
Term	Coef.					
Constant	406.30					
rpm	−0.019					
s/mm	−64.01					
Ct Pt	8.47					

distributed with null average and constant standard deviation. Moreover, the regression model fits the data very well since the high p value related to the lack of fit (0.782) is just a consequence of the interaction term omission. Experimental data of ultimate strength are shown in Table 5. The analysis of variability related to the experimental data of ultimate strength is shown in Table 6.

It can be seen that only two effects could be considered significant: rpm with a p value of 0.059 and the inverse of the travel speed with a p value of 0.006; the interaction effect seems not to be noticeable. Either curvature could be considered significant. The weighted ANOVA related to the experimental data of ultimate strength is shown in Table 7. The regression model presented has been reduced by

Table 5: Ultimate strength experimental responses.

rpm	s/mm	Us1	Us2	Us3	Us4	Std. US	Dim	Avg. US	WGTS_ADJ
1377.5	0.267	502.0	480.0	484.0	—	11.719	3	488.667	0.0324
2222.5	0.267	431.0	432.5	460.2	—	16.443	3	441.233	0.0081
1377.5	0.533	444.6	419.5	478.0	—	29.348	3	447.367	0.0026
2222.5	0.533	435.6	452.0	285.0	392	75.160	4	391.150	0.0008
1800.0	0.400	491.0	501.4	449.0	—	27.743	3	480.467	0.0046
1800.0	0.400	496.6	492.5	428.6	—	38.131	3	472.567	0.0046
1800.0	0.400	456.0	485.7	483.3	—	16.498	3	475.000	0.0046
1800.0	0.400	475.7	451.8	494.0	—	21.162	3	473.833	0.0046
1800.0	0.400	472.0	466.8	514.0	—	25.881	3	484.267	0.0046

Table 6: Results of ultimate strength analysis of variability.

Regression estimated effects and coefficients for natural log of std. US ratio (coded units)						
Term	Effect	Effect	Coef.	SE coef.	T	p
Constant	—	—	3.2266	0.0909	35.48	0.0
rpm	0.6428	1.902	0.3214	0.1317	2.44	0.059
s/mm	1.2221	3.394	0.6111	0.1317	6.64	0.006
rpm ∗ s/mm	0.3041	1.355	0.1520	0.1317	1.15	0.301
	$R^2 = 87.80\%$		$R^2(\text{adj}) = 80.48\%$			
Analysis of variance for natural log of std. US						
Source	DF	Seq. SS	Adj. SS	Adj. MS	F	p
Main effects	2	6.6109	5.8970	2.9485	15.46	0.007
2-Way interactions	1	0.2540	0.2540	0.2540	1.33	0.301
Residual error	5	0.9537	0.9537	0.1907	—	—
Curvature	1	0.0037	0.0037	0.0037	0.02	0.907
Pure error	4	0.9500	0.9500	0.2375	—	—
Total	8	7.8187	—	—	—	—

Table 7: Results of ultimate strength weighted analysis of variance.

Estimated effects and coefficients for avg. US (coded units)					
Term	Effect	Coef.	SE coef.	T	p
Constant	—	442.97	2.973	148.99	0.0
rpm	−48.23	−24.12	1.860	−12.96	0.0
s/mm	−43.49	−21.75	2.798	−7.77	0.001
Ct Pt	—	34.26	3.629	9.44	0.0
	$S = 0.3170$	$R^2 = 97.93\%$	$R^2(\text{adj}) = 96.68\%$		
Analysis of variance for avg. US (coded units)					
Source	DF	Seq. SS	Adj. SS	Adj. MS	F	p
Main effects	2	14.7680	23.677	11.838	117.76	0.0
Curvature	1	8.9605	8.9605	8.9605	89.13	0.0
Residual error	5	0.5027	0.5027	0.1005	—	—
Lack of fit	1	0.0464	0.0464	0.0464	0.41	0.558
Pure error	4	0.4563	0.4563	0.1141	—	—
Total	8	24.2317	—	—	—	—
Estimated coefficients for avg. US using data in uncoded units						
Term	Coef.					
Constant	611.11					
rpm	−0.057					
s/mm	−163.52					
Ct Pt	34.26					

removing the interaction effect since a previous analysis proved its negligibility. In fact, the value of F related to the interaction effect is 0.41 corresponding to a p value of 0.558.

The analysis shows a significant curvature p value, whose value is less than 0.001, a main effect p value less than 0.001 ensuring a huge significant influence; specifically, the p value related to rpm is less than 0.001 and the p value related to TS^{-1} is 0.001. Both the effects can be considered very significant. Regression model coefficients are estimated as shown in Table 7. It was also performed a residuals analysis that seems to verify the hypothesis made on the residuals, so they can be assumed to be normally distributed with null average and constant standard deviation. By the way, the regression model cannot fit well the data, even if the p value

related to the lack of fit is very high, since the adopted design cannot allow second-order estimate effects being significant in this case.

As for the nugget zone, a 2^2 factorial design with two centre points and three repeated measurements was carried out for the elongation. Experimental data of yield strength are shown in Table 8.

In this case, a simple ANOVA was carried out since the analysis of variability did not show any significant effect. Reliance on this consideration would deem the weights negligible. The ANOVA related to the experimental data of elongation is shown in Table 9.

The analysis shows a curvature p value of 0.070 that proves its presence; the main effect p value is 0.051; specifically, the p value related to rpm is 0.037 which is significant. The p value related to TS^{-1} is 0.198, which is not significant. The residuals can be assumed to be normally distributed, with null average and constant standard deviation. An important point is that the high p value related to the curvature proves even a lack of fit of the regression model. Looking data of ultimate strength, yield strength, and elongation relative of the analysis of variance, it can be seen that the influence effects are not significant.

Regarding the optimization of the response surface related to the yield strength, which is the main mechanical property of interest, an algorithm of steepest ascent to the yield strength response of the nugget zone was proposed. Assuming that $x_1 = x_2 = \cdots = x_k = 0$, where $i = 1, 2, \ldots, k$ identifies the factors and $[-1; 0; 1]$ are the coded variables identifying the lower, the centre, and the upper level of the factors, respectively, the algorithm procedure can be described according to the following procedure: defining the step length for one of the process variables and the step length of the other variables can be defined by using equation (1). Finally, turning the step length Δx_i from the coded variable into natural variables.

This algorithm can be applied only when the regression model is of the first order and does not include interactions. Runs obtained by implementing the aforementioned algorithm are shown in Table 10:

$$\Delta x_i = \frac{\beta_i}{\beta_j \Delta x_j}, \quad \text{with } i = 1, 2, \ldots, k, \ i \neq j. \tag{1}$$

The results are similar to those expected, and this ascertainment guarantees the reliability of the previous analysis. The average of the yield strength has increased from a value of 363.33 MPa (point: 1377.5 rpm; 0.267 s/mm) to values of 399.25 MPa (point: 1250 rpm; 0.241 s/mm) and 395.8 MPa (point: 1150 rpm; 0.213 s/mm). The region where the two last points are set is the optimum region; a new investigation using a central composite design would have been necessary to determine the exact position of the yield strength optimum point. Following the next steps of the steepest path, the yield strength decreases, which suggests that the steepest path is leaving from the optimum region. A similar behaviour is acted also by the ultimate strength, but steepest yield strength of the nugget zone path is even one of the improvement directions of yield and ultimate strength of the heat-affected zone. Seemingly, the mechanical properties of the HAZ improve markedly when the process gets colder and colder.

Table 8: Elongation experimental responses.

rpm	s/mm	El1	El2	El3	Std. El	Dim	Avg. El
1377.5	0.267	31.5	30.5	32.0	0.764	3	31.333
2222.5	0.267	9.0	9.0	15.0	3.464	3	11.000
1377.5	0.533	23.0	30.5	27.5	3.775	3	27.000
2222.5	0.533	11.5	4.5	9.0	3.547	3	8.333
1800.0	0.400	33.6	25.0	32.0	4.574	3	30.200
1800.0	0.400	26.0	28.0	31.0	2.517	3	28.333

As for the shear testing, the results showed averaged failure loads, since three specimens were tested for each run. In Table 11, a summary of averaged failure loads is presented.

According to the tensile testing results, the runs corresponding to the first two steepest ascent algorithms show the best performances for yield strength, especially the run (1150 rpm; 0.213 s/mm) which had an averaged failure load of 10125.16 N. Those failures occur always in the nugget zone explaining the correlation between tensile and shear testing.

Vickers microhardness measurements, which were carried out from the centre of the welding along the cross section passing through HAZ, TMAZ, and nugget zone, are shown in Figure 4.

The results reveal a switch of the best mechanical behaviour zones, from welds showing better hardness performances in the nugget zone to welds showing better hardness performances in the HAZ. Looking at the welds carried out by setting rpm equal to 1050 and TS^{-1} equal to 0.184 s/mm and the ones obtained with rpm equal to 1150 and TS^{-1} equal to 0.213 s/mm (Figure 4), the switch in hardness performances confirms the results already obtained with tensile testing. In fact, as well as tensile testing has held up when the runs get very cold (namely, the following runs: rpm = 950; $TS^{-1} = 0.155$ s/mm, rpm = 1050; $TS^{-1} = 0.184$ s/mm), improved mechanical behaviour in the HAZ exceeds nugget zone performance. Thus, microhardness testing confirms the same trend of tensile testing.

Optical investigations included the study of the oxide film; this kind of defect, which is a feature for friction stir welding technology, is commonly called hook defect because of its shape. Hook defects must be taken seriously since they represent cross-section thinning, and for this reason, they may explain shear testing results [31]. Hook's distances are shown in Table 12.

This study does not contain statistical evidence for hook's distance and shear tests correlation; in fact, a linear regression analysis showed a very low coefficient of determination ($R^2 = 0.102$ and $R^2(\text{adj}) = 0$) and a very high ANOVA p value ($F = 0.68$; p value = 0.44).

As for the grain size number of the nugget zone, the results are shown in Table 13.

It can be seen a decrease in grain size for runs featured by high heat generation. A regression analysis between grain size estimates and heat index was carried out as proof. Heat index is considered as a measurement of heat

Table 9: Results of elongation analysis of variance (nugget zone).

Estimated effects and coefficients for avg. El (coded units)					
Term	Effect	Coef.	SE coef.	T	p
Constant	—	19.417	0.5612	34.60	0.018
rpm	−19.500	−9.750	0.5612	−17.37	0.037
s/mm	−3.500	−1.750	0.5612	−3.12	0.198
rpm ∗ s/mm	0.833	0.417	0.5612	0.74	0.593
Ct Pt	—	9.850	1.089	9.04	0.070
	$S = 0.619324$	$R^2 = 99.82\%$	$R^2(\text{adj}) = 99.09\%$		
Analysis of variance for avg. El (coded units)					
Source	DF	Seq. SS	Adj. SS	Adj. MS	F	p
Main effects	2	179.25	149.80	74.90	195.26	0.051
2-Way interactions	1	0.256	0.211	0.211	0.55	0.593
Curvature	1	31.37	31.37	31.37	81.80	0.070
Residual error	1	0.384	0.384	0.384	—	—
Pure error	1	0.384	0.384	0.84	—	—
Total	5	211.26	—	—	—	—
Estimated coefficients for avg. El using data in uncoded units						
Term	Coef.					
Constant	71.56					
rpm	−0.026					
s/mm	−23.51					
rpm ∗ s/mm	0.0074					
Ct Pt	9.85					

Table 10: Yield strength, ultimate strength, and elongation experimental responses performed along the steepest ascent direction (summarized data for nugget and HAZ).

rpm	s/mm	Avg. YS	Avg. US	Avg. El
Nugget				
1250	0.241	399.25	511.8	28.75
1150	0.213	395.8	507.9	26.36
1050	0.184	339.33	453	25.25
950	0.155	368.67	475.6	25.23
HAZ				
1250	0.241	370	482.3	19.8
1150	0.213	368	474.5	20.17
1050	0.184	386	491	21.4
950	0.155	405.7	506.25	21.45

Table 11: Shear testing results of averaged failure loads.

rpm	s/mm	Shear testing results (N)
950	0.155	7433.596
1050	0.184	7531.358
1150	0.213	10125.16
1250	0.241	8394.355
1377.5	0.533	5708.624
1377.5	0.267	7768.978
1800	0.25	7001.34
2222.5	0.533	6682.956
2222.5	0.267	4074.074

generated during welding, as the higher the index, the higher is the heat generated. It was defined by using the following equation:

$$\text{HI} = \frac{\text{rpm}^2}{(\text{inch/min}) \times 10000}. \quad (2)$$

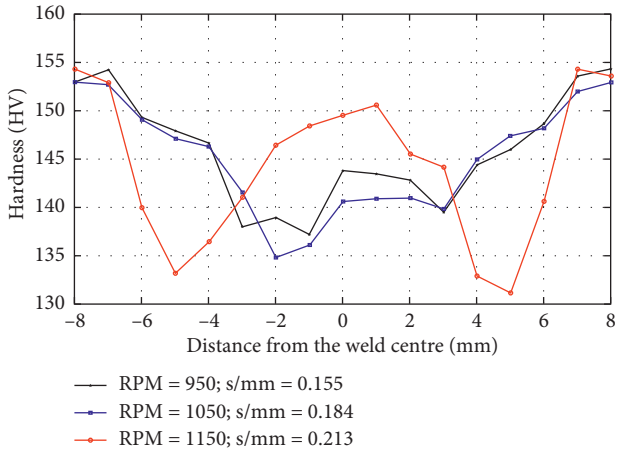

Figure 4: Vickers microhardness measurement results.

Table 12: Minimum hook distances measured on advancing (AS) and retreating (RS).

rpm	s/mm	Loaded AS thickness (mm)	Loaded RS thickness (mm)
950	0.155	0.12	0.12
1050	0.184	0.11	0.12
1150	0.213	0.114	0.116
1250	0.241	0.09	0.12
1377.5	0.533	0.074	0.12
1377.5	0.267	0.032	0.12
2222.5	0.533	0.044	0.12
2222.5	0.267	0.08	0.12

The coefficient of determination presented a high value ($R^2 = 0.68$, $R^2(\text{adj}) = 0.63$), which suggests a good correlation between the two parameters, as well the analysis of variance as

Table 13: ASTM grains size number versus heat index regression.

rpm	s/mm	G	HI
950	0.155	8.54	5.710
1050	0.184	8.60	8.350
1150	0.213	8.66	11.664
1250	0.241	8.72	15.749
1377.5	0.267	8.78	42.841
1377.5	0.533	8.84	21.421
1800	0.25	8.90	54.864
2222.5	0.267	8.96	55.762

proof of a significant influence of the heat index on grain size showing a p value of 0.012. In other words, these analyses seem to ensure this assertion: "As big is the heat generation as big is the grain size in the Nugget Zone." The mechanical behaviour of the welds is explained by regression analysis between hardness Vickers tests and grain size. Such an analysis revealed a lack of correlation between the two properties, thus disagreeing with the Hall–Petch rule. So, the causes of the mechanical behaviour should be found in the differences of the weld microstructure; i.e., different temporal thermal profiles produce different precipitate compositions, where some are more hardened than others [22, 32, 33].

4. Conclusions

In this study, a procedure to optimize the mechanical behaviour of friction stir welded joints was developed. The yield strength was chosen as a factor of interest, and its response was optimized by using a response surface method. This method, which consisted of a central composite design and a subsequent steepest ascent algorithm, provided for optimal yield strength surface. Tensile tests on base metal specimens were conducted with benchmarking measures obtained from processed samples proving the high performance of FSW technology. The best performances, which were evaluated choosing the minimum value between HAZ and nugget zone ratio for both yield and ultimate strength, were found under these welding conditions: rpm = 1250 and $TS^{-1} = 0.241$ s/mm. Shear testing confirmed the results provided by tensile tests. Hook's defect was studied, and the grain size of the nugget zone was estimated.

Data Availability

The data used to support the findings of this study are included within the article.

Conflicts of Interest

The authors declare that they have no conflicts of interest.

References

[1] V. M. Magalhães, C. Leitão, and D. M. Rodrigues, "Friction stir welding industrialisation and research status," *Science and Technology of Welding and Joining*, vol. 23, no. 5, pp. 400–409, 2017.

[2] X. Liu, S. Lan, and J. Ni, "Analysis of process parameters effects on friction stir welding of dissimilar aluminum alloy to advanced high strength steel," *Materials & Design*, vol. 59, pp. 50–62, 2014.

[3] R. Nandan, T. Debroy, and H. Bhadeshia, "Recent advances in friction-stir welding-process, weldment structure and properties," *Progress in Materials Science*, vol. 53, no. 6, pp. 980–1023, 2008.

[4] Y. S. Sato, M. Urata, and H. Kokawa, "Parameters controlling microstructure and hardness during friction-stir welding of precipitation-hardenable aluminum alloy 6063," *Metallurgical and Materials Transactions A*, vol. 33, no. 3, pp. 625–635, 2002.

[5] A. Ali, M. W. Brown, C. A. Rodopoulos, and S. Gardiner, "Characterization of 2024-T351 friction stir welding joints," *Journal of Failure Analysis and Prevention*, vol. 6, no. 4, pp. 83–96, 2006.

[6] M. W. Mahoney, C. G. Rhodes, J. G. Flintoff, W. H. Bingel, and R. A. Spurling, "Properties of friction-stir-welded 7075 T651 aluminum," *Metallurgical and Materials Transactions A*, vol. 29, no. 7, pp. 1955–1964, 1998.

[7] R. Nandan, G. G. Roy, T. J. Lienert, and T. Debroy, "Three-dimensional heat and material flow during friction stir welding of mild steel," *Acta Materialia*, vol. 55, no. 3, pp. 883–895, 2007.

[8] H. J. Liu, H. Fujii, M. Maeda, and K. Nogi, "Tensile properties and fracture locations of friction-stir-welded joints of 2017-T351 aluminum alloy," *Journal of Materials Processing Technology*, vol. 142, no. 3, pp. 692–696, 2003.

[9] R. F. Gunst, "Response surface methodology: process and product optimization using designed experiments," *Technometrics*, vol. 38, no. 3, pp. 284–286, 1996.

[10] J. Antony, "Simultaneous optimisation of multiple quality characteristics in manufacturing processes using taguchi's quality loss function," *International Journal of Advanced Manufacturing Technology*, vol. 17, no. 2, pp. 134–138, 2001.

[11] T. V. Sibalija and V. D. Majstorovic, "An integrated approach to optimise parameter design of multi-response processes based on Taguchi method and artificial intelligence," *Journal of Intelligent Manufacturing*, vol. 23, no. 5, pp. 1511–1528, 2010.

[12] M. J. Anderson, "A new method for non-parametric multivariate analysis of variance," *Austral Ecology*, vol. 26, no. 1, pp. 32–46, 2001.

[13] W. B. Schaufeli, M. Salanova, V. González-romá, and A. B. Bakker, "The measurement of engagement and burnout: a two sample confirmatory factor analytic approach," *Journal of Happiness Studies*, vol. 3, no. 1, pp. 71–92, 2002.

[14] N. Alagumurthi, K. Palaniradja, and V. Soundararajan, "Optimization of grinding process through design of experiment (DOE)-a comparative study," *Materials and Manufacturing Processes*, vol. 21, no. 1, pp. 19–21, 2006.

[15] W. Chen, J. K. Allen, K.-L. Tsui, and F. Mistree, "A procedure for robust design: minimizing variations caused by noise factors and control factors," *Journal of Mechanical Design*, vol. 118, no. 4, p. 478, 1996.

[16] G. Vicente, A. Coteron, M. Martinez, and J. Aracil, "Application of the factorial design of experiments and response surface methodology to optimize biodiesel production," *Industrial Crops and Products*, vol. 8, no. 1, pp. 29–35, 1998.

[17] B. K. Rout and R. K. Mittal, "Parametric design optimization of 2-DOF R-R planar manipulator-A design of experiment approach," *Robotics and Computer-Integrated Manufacturing*, vol. 24, no. 2, pp. 239–248, 2008.

[18] A. E. Bryson and W. F. Denham, "A steepest-ascent method for solving optimum programming problems," *Journal of Applied Mechanics*, vol. 29, no. 2, p. 247, 1962.

[19] M. Jones, P. Heurtier, C. Desrayaud, F. Montheillet, D. Allehaux, and J. Driver, "Correlation between microstructure and microhardness in a friction stir welded 2024 aluminium alloy," *Scripta Materialia*, vol. 52, no. 8, pp. 693–697, 2005.

[20] G. Liu, L. E. Murr, C.-S. Niou, J. C. McClure, and F. R. Vega, "Microstructural aspects of the friction-stir welding of 6061-T6 aluminum," *Scripta Materialia*, vol. 37, no. 3, pp. 355–361, 1997.

[21] G. D'Urso and C. Giardini, "The influence of process parameters and tool geometry on mechanical properties of friction stir welded aluminum lap joints," *International Journal of Material Forming*, vol. 3, no. 1, pp. 1011–1014, 2010.

[22] Y. S. Sato, M. Urata, H. Kokawa, and K. Ikeda, "Hall-Petch relationship in friction stir welds of equal channel angular-pressed aluminium alloys," *Materials Science and Engineering: A*, vol. 354, no. 1-2, pp. 298–305, 2003.

[23] P. M. G. P. Moreira, T. Santos, S. M. O. Tavares, V. Richter-Trummer, P. Vilaça, and P. M. S. T. de Castro, "Mechanical and metallurgical characterization of friction stir welding joints of AA6061-T6 with AA6082-T6," *Materials & Design*, vol. 30, no. 1, pp. 180–187, 2009.

[24] L. Commin, M. Dumont, J.-E. Masse, and L. Barrallier, "Friction stir welding of AZ31 magnesium alloy rolled sheets: influence of processing parameters," *Acta Materialia*, vol. 57, no. 2, pp. 326–334, 2009.

[25] W. Zhang, Y. Shen, Y. Yan, and R. Guo, "Dissimilar friction stir welding of 6061 Al to T2 pure Cu adopting tooth-shaped joint configuration: microstructure and mechanical properties," *Materials Science and Engineering: A*, vol. 690, pp. 355–364, 2017.

[26] R. S. Mishra and Z. Y. Ma, "Friction stir welding and processing," *Materials Science and Engineering: R: Reports*, vol. 50, no. 1-2, pp. 1–78, 2005.

[27] A. Murphy, M. Price, R. Curran, and P. Wang, "Integration of strength and process modeling of friction-stir-welded fuselage panels," *Journal of Aerospace Computing, Information, and Communication*, vol. 3, no. 4, pp. 159–176, 2006.

[28] A. V. Sergueeva, J. Zhou, B. E. Meacham, and D. J. Branagan, "Gage length and sample size effect on measured properties during tensile testing," *Materials Science and Engineering: A*, vol. 526, no. 1-2, pp. 79–83, 2009.

[29] M. Ahmadi, F. Vahabzadeh, B. Bonakdarpour, E. Mofarrah, and M. Mehranian, "Application of the central composite design and response surface methodology to the advanced treatment of olive oil processing wastewater using Fenton's peroxidation," *Journal of Hazardous Materials*, vol. 123, no. 1–3, pp. 187–195, 2005.

[30] W. S. Cleveland and S. J. Devlin, "Locally weighted regression: an approach to regression analysis by local fitting," *Journal of the American Statistical Association*, vol. 83, no. 403, pp. 596–610, 1988.

[31] W. Li, J. Li, Z. Zhang, D. Gao, W. Wang, and C. Dong, "Improving mechanical properties of pinless friction stir spot welded joints by eliminating hook defect," *Materials & Design (1980–2015)*, vol. 62, pp. 247–254, 2014.

[32] N. Dialami, M. Chiumenti, M. Cervera, and C. Agelet de Saracibar, "Challenges in thermo-mechanical analysis of friction stir welding processes," *Archives of Computational Methods in Engineering*, vol. 24, no. 1, pp. 189–225, 2016.

[33] M. M. Attallah, C. L. Davis, and M. Strangwood, "Microstructure-microhardness relationships in friction stir welded AA5251," *Journal of Materials Science*, vol. 42, no. 17, pp. 7299–7306, 2007.